International Journal of Civil Engineering

Structure - Steel

Technical Note

A dynamic model for the interaction of the cable bridge and train system

M.M. Jalili[1,*], A.H. Orafa[2]

Received: December 2013, Revised: April 2014, Accepted: December 2014

Abstract

The vibration of cable-stayed bridges subjected to the passage of high-speed trains is studied in this article. The moving train includes a number of wagons, each of which is modeled as a four-axle system possessing 48 degrees of freedom. The car model is nonlinear and three-dimensional and includes nonlinear springs and dampers of primary and secondary suspensions, dry friction between different parts and also clearances and mechanical stops. Two parallel rails of the track are modeled as Euler-Bernoulli beams on elastic points as rail pads. The rail irregularities are assumed to be stationary random and ergodic processes in space, with Gaussian amplitude probability densities and zero mean values. The bridge deck is modeled as a plate supported by some cables. The current model is validated using several numerical models reported in the literature of the earlier researcher.

Keywords: *Rail vehicle dynamics, Euler-Bernoulli beam, Levy method, Random rail irregularities.*

1. Introduction

To meet the economic, social and recreational needs of the community for safe and efficient transportation systems, more and more cable bridges have been built throughout the world. Cable-stayed bridges were often constructed for crossing wide rivers and deep valleys or existing urban structures because of their economic and aesthetic advantages. The investigation of the cable bridge vibration under moving train using different models has been widely reported in the literature. For most of the previous studies the cable-stayed bridge has been modeled as a planar system. Au et al. [1] used 2-D model to study bridge vibration due to random rail irregularities. They studied effects of number of random samples, damping, class of railway, track quality and initial motion of train vehicles on bridge vibration. Using a planar model for vehicle/ bridge, the vibration reduction of cable bridges excited by high-speed trains is studied by Yau and Yang [2]. 2-D models cannot simulate lateral vibration of the bridge. In addition wagon derailment and hunting vibration cannot be investigated by these models.

For the 3-D models, the finite element method has been used as the main tool for bridge simulation. For instance, using FEM, the vibration of coupled train and cable-stayed bridge systems in cross winds has been investigated by Xu et al. [3]. Also, the dynamic stability of trains moving over bridges shaken by earthquakes has been studied by Yang and Wu [4]. Using this model the maximum allowable speed for the train to run safely has been obtained under the specified ground acceleration.

In this article, an analytical solution is presented for simulation of the coupled system. A 3-D model of the cable-stayed bridge, rails and passenger wagon is developed. Equations of motion of this model are derived. Using the proposed model, the effects of wagon parameters, lateral position of the rails and the rail irregularities on vehicle/track dynamics are studied.

2. System Model

2.1. The train model

A 3-D model of a 2- axle passenger wagon with 48 DOF is developed here. All parts of primary and secondary suspension systems with their nonlinear characteristics, friction between moving elements, the effect of wheel flange contact with the rail, wheel rail nonlinear contact forces, kinematics constraint of bogie center plate, and the contact forces between side pads and bogie frame are considered in this model. Schematic of wagon model is shown in Figure 1. Basic dynamic parameters of wagon are presented in Table 1.

** Corresponding author: jalili@yazd.ac.ir*
1 Assistant professor, Mechanical Engineering Department, Yazd University, PO Box 89195-741, Yazd, Iran
2 PhD Student, Mechanical Engineering Department, Yazd University, PO Box 89165-741, Yazd, Iran

[DOI: 10.22068/IJCE.13.3.347]

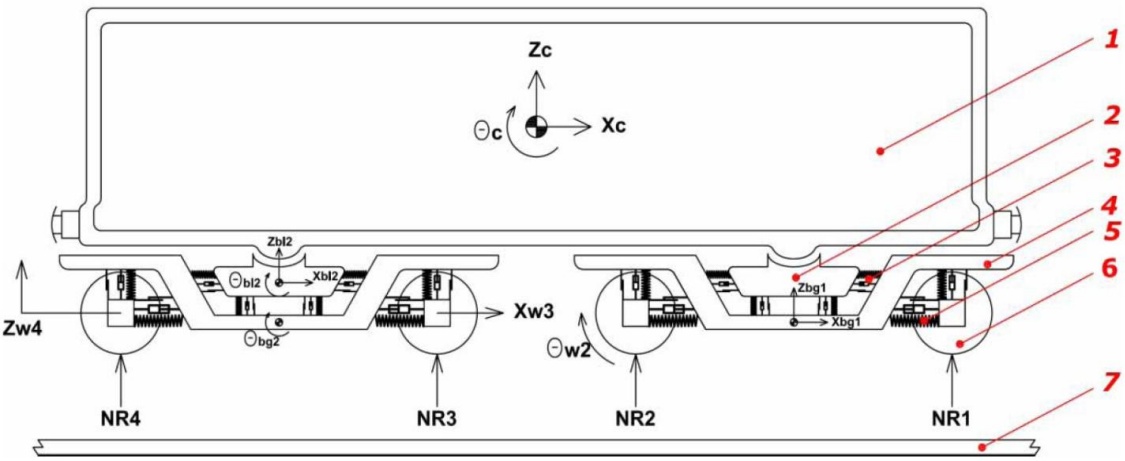

Fig. 1 Schematic view of the wagon model: (1) wagon body, (2) bolster, (3) secondary suspension system, (4) bogie, (5) primary suspension system, (6) wheelset, and (7) rail

Table 1 Main parameters of the car body

Notation	Parameter	Value
	Wagon body	
M_c	Wagon body mass	20000 kg
I_{cx}	Wagon mass moment of inertia about X axis	32268 kg m^2
I_{cy}	Wagon mass moment of inertia about Y axis	1125000 kg m^2
I_{cz}	Wagon mass moment of inertia about Z axis	1125000 kg m^2
	Bolster	
M_{bol}	Bolster body mass	630 kg
I_{bolx}	Bolster mass moment of inertia about X axis	160 kg m^2
I_{boly}	Bolster mass moment of inertia about Y axis	100 kg m^2
I_{bolz}	Bolster mass moment of inertia about Z axis	160 kg m^2
	Bogie	
M_{bog}	Bogie body mass	500 kg
I_{bogx}	Bogie mass moment of inertia about X axis	250 kg m^2
I_{bogy}	Bogie mass moment of inertia about Y axis	150 kg m^2
I_{bogz}	Bogie mass moment of inertia about Z axis	300 kg m^2
	wheelset	
M_w	Wheelset body mass	1180 kg
I_{wx}	Wheelset mass moment of inertia about X axis	680 kg m^2
I_{wy}	Wheelset mass moment of inertia about Y axis	73 kg m^2
I_{wz}	Wheelset mass moment of inertia about Z axis	680 kg m^2
r_w	Wheel radius	0.46 m
	Primary Suspension	
K_z	Vertical stiffness	6500 kN/m
K_x, K_y	Lateral and longitudinal Stiffness	6500 kN/m
C_z	Vertical damping	10 kNs/m
C_x, C_y	Lateral and longitudinal damping	9 kNs/m
	Secondary Suspension	

[DOI: 10.22068/IJCE.13.3.347]

K_z	Vertical stiffness	2555 kN/m
K_x, K_y	Lateral and longitudinal Stiffness	1500 kN/m
C_z	Vertical damping	30 kNs/m
C_x, C_y	Lateral and longitudinal damping	20 kNs/m

Considering the nature of this problem, use of 3-dimensional wheelset model is essential. Determination of the correct contact point between wheel and rail and the exact value of the contact force between the two members are the major issues in 3-D modeling of the wheelset. To determine normal contact force between the wheel and rail, a flexible wheel–rail contact model based on semi-Hertzian methods and the virtual penetration theory has been used [5]. Also in order to determine the tangential forces, the FASTSIM algorithm has been used.

The connection link between wagons is considered to be hooks and draft gears [6]. The buffers at each side of the cars have also been included in the model to account for the absorption of the excess energy in inter-wagon force transmissions (Fig. 2). The degrees of freedom for the wagon components are listed in Table 2.

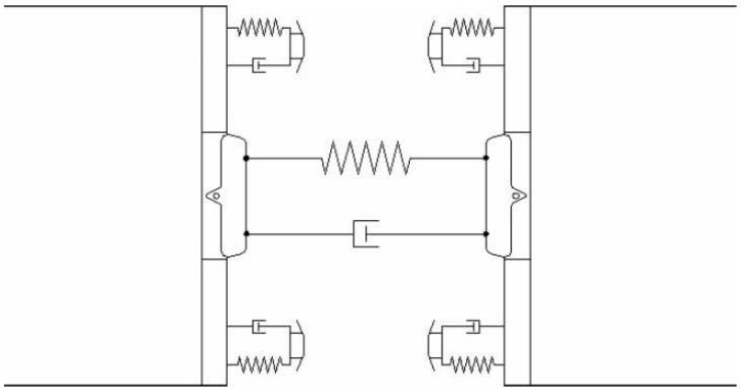

Fig. 2 Model of connection between wagons

Table 2 Degrees of freedom of each part of the wagon

	longitudinal	lateral	vertical	roll	pitch	yaw
Car body	*	*	*	*	*	*
Bogie frame	*	*	*	*	*	*
Bolster	-	-	-	*	*	*
Wheel set	*	*	*	*	*	*

Table 3 A_v, coefficient related to line grade[1]

Line Grade	A_v	Line Grade	A_v
1	15.52×10^{-8}	4	2.75×10^{-8}
2	8.84×10^{-8}	5	1.55×10^{-8}
3	4.91×10^{-8}	6	0.88×10^{-8}

2.2. The bridge model

Figure 3 shows the bridge model adopted in the present study. The bridge deck is modeled as a plate supported by some cables. Also the bridge towers are modeled as a beam in lateral and a bar in vertical direction. Rails are modeled as Euler-Bernoulli beams on elastic points as rail pads (Fig. 4).

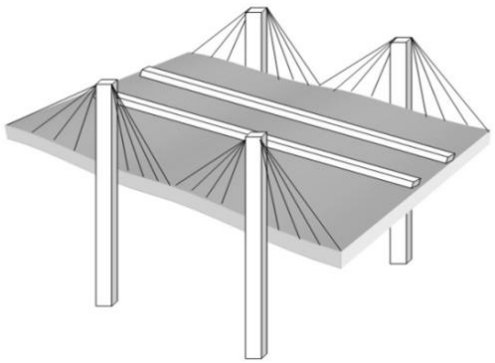

Fig. 3 3D model of the bridge

[DOI: 10.22068/IJCE.13.3.347]

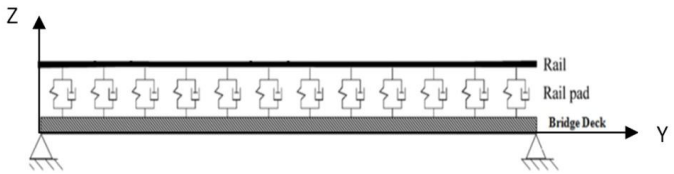

Fig. 4 Side view of the system model

2.3. Irregularities model

Rail irregularities generally have a random distribution, and are considered as one of the major source of wagon vibration and wheelset derailment. The major causes of these irregularities are: incompatible substrate conditions, weather conditions, rail age and excessive train commutation on rails [7].

The random rail irregularities are assumed to be stationary random and ergodic processes in space, with Gaussian amplitude probability densities and zero mean values. They are characterized by their respective one-sided power spectral density functions $G_{rr}(\omega)$ where ω is the route frequency. Fryba [8] has summarized various commonly used power spectral density functions. In the present study, the power spectral density functions based on the results of measurements on US railway tracks is adopted, with the empirical formula for evaluation of irregularities as:

$$G_{rr}(\omega)=\frac{A_v\omega_2^2\left(\omega^2+\omega_1^2\right)}{\omega^4\left(\omega^2+\omega_2^2\right)} \tag{1}$$

Where $\omega_1=0.0233\,m^{-1}$ and $\omega_2=0.131m^{-1}$ and the parameter A_v is a coefficient related to line grade, as shown in Table [1].

A sample function of rail irregularities can be generated numerically using the following series:

$$r^d(x)=\sum_{k=1}^{N}a_k\cos\left(\omega_k x+\varphi_k\right) \tag{2}$$

Where a_k is the amplitude of the cosine wave, ω_k is a frequency within the interval $\left[\omega_l,\omega_u\right]$ in which the power spectral density function is defined, ϕ_k is a random phase angle with uniform probability distribution in the interval $\left[0,2\pi\right]$, x is the global coordinate measured from the start of the rail section and N is the total number of terms used to generate the rail irregularities function. The parameters a_k and ω_k are computed using equations Eq.(3) and Eq.(4):

$$a_k=2\sqrt{G_{rr}(\omega_k)\Delta\omega} \tag{3}$$

$$\omega_k=\omega_l+\left(k-\tfrac{1}{2}\right)\Delta\omega \tag{4}$$

$$\Delta\omega=\left(\omega_u-\omega_l\right)/N \tag{5}$$

In which ω_u and ω_l are the upper and lower limits of the frequency, and N is a sufficiently large integer. Using equations Eq. (1-5), random rail irregularities in each line grade can be generated.

3. Equations of Motion

3.1. Deck equation of motion

Describing the bridge deck as a plate, the vertical vibration of the bridge deck is given by:

$$\frac{\partial^4 w_s(x,y,t)}{\partial x^4}+2\frac{\partial^4 w_s(x,y,t)}{\partial x^2\partial y^2}+\frac{\partial^4 w_s(x,y,t)}{\partial y^4}+\frac{\rho_s h_s}{D_s}\frac{\partial^2 w_s(x,y,t)}{\partial t^2}=-\frac{1}{D_s}\left(F_{ts}^z+\sum_{k=1}^{K}F_{r_k s}\right) \tag{6}$$

Where

$$F_{r_k s}=-\sum_{f=1}^{N_f}[K_f(w_s(x_f,y_{r_k},t)-w_{r_k}(x_f,t))+C_f(\dot{w}_s(x_f,y_{r_k},t)-\dot{w}_{r_k}(x_f,t))]\times\delta(x-x_f)\delta(y-y_{r_k}) \tag{7}$$

$$\begin{aligned}F_{ts}^z=&\\ &\sum_{c=1}^{N_C}\frac{E_cA_c}{L_c}(C_{11}\delta(y)+C_{33}\delta(y-b))\delta(x-x_c)\sin(\alpha_c)+\\ &\sum_{c=N_C+1}^{2N_C}\frac{E_cA_c}{L_c}(C_{21}\delta(y)+C_{43}\delta(y-b))\delta(x-x_c)\sin(\alpha_c)+\\ &\sum_{c=2N_C+1}^{3N_C}\frac{E_cA_c}{L_c}(C_{12}\delta(y)+C_{34}\delta(y-b))\delta(x-x_c)\sin(\alpha_c)+\\ &\sum_{c=3N_C+1}^{4N_C}\frac{E_cA_c}{L_c}(C_{22}\delta(y)+C_{44}\delta(y-b))\delta(x-x_c)\sin(\alpha_c)\end{aligned} \tag{8}$$

[DOI: 10.22068/IJCE.13.3.347]

in which

$$
\begin{aligned}
C_{1k} &= -w_s(x_c,0,t)\sin(\alpha_c) + w^x_{t_k}(H)\cos(\alpha_c) + w^z_{t_k}(H)\sin(\alpha_c)\\
C_{2k} &= -w_s(x_c,0,t)\sin(\alpha_c) - w^x_{t_k}(H)\cos(\alpha_c) + w^z_{t_k}(H)\sin(\alpha_c)\\
C_{3k} &= -w_s(x_c,b,t)\sin(\alpha_c) + w^x_{t_k}(H)\cos(\alpha_c) + w^z_{t_k}(H)\sin(\alpha_c)\\
C_{4k} &= -w_s(x_c,b,t)\sin(\alpha_c) - w^x_{t_k}(H)\cos(\alpha_c) + w^z_{t_k}(H)\sin(\alpha_c)
\end{aligned}
\qquad (9)
$$

And

$$D_s = \frac{E_s h_s^{\,3}}{12(1-\nu_s^{\,2})} \qquad (10)$$

Using Levy method, the solution of homogenous form of Eq. (6) can be expressed as [9]:

$$w_s(x,y,t) = X_m(x)Y_{mn}(y)T_{mn}(t) = \sin(\frac{m\pi}{a}x)Y_{mn}(y)T_{mn}(t) \qquad (11)$$

Substituting Eq. (11) into homogenous form of Eq. (6) yields:

$$[(\frac{m\pi}{a})^4 YT - 2(\frac{m\pi}{a})^2 Y^{(2)}_{mn}T + Y^{(4)}_{mn}T + \frac{\rho_s h_s}{D_s}Y\ddot{T}_{mn}]\sin(\frac{m\pi}{a}x) = 0 \qquad (12)$$

Using Separation of variables, vibration frequencies can be found as:

$$-\frac{D_s}{\rho_s h_s}[(\frac{m\pi}{a})^4 - 2(\frac{m\pi}{a})^2\frac{Y^{(2)}_{mn}}{Y_{mn}} + \frac{Y^{(4)}_{mn}}{Y_{mn}}] = \frac{\ddot{T}_{mn}}{T_{mn}} = -\omega_{mn}^{\,2} \qquad (13)$$

and finally a differential equation can be derived as follows:

$$Y^{(4)}_{mn} - 2(\frac{m\pi}{a})^2 Y^{(2)}_{mn} - (\frac{\rho_s h_s}{D_s}\omega_{mn}^{\,2} - (\frac{m\pi}{a})^4)Y_{mn} = 0 \qquad (11)$$

The bending moments and the shearing forces for the two free edges at $y=0$ and $y=b$ are equal to zero. So the boundary conditions are:

$$M_y\big|_{y=0,b} = D_s(\frac{\partial^2 w_s}{\partial y^2} + \nu_s\frac{\partial^2 w_s}{\partial x^2})\Big|_{y=0,b} = D_s(Y^{(2)}_{mn} - \nu_s(\frac{m\pi}{a})^2 Y_{mn})\Big|_{y=0,b} = 0 \qquad (15)$$

$$Q_y\big|_{y=0,b} = D_s(\frac{\partial^3 w_s}{\partial y^3} + (2-\nu_s)\frac{\partial^3 w_s}{\partial x^2\partial y})\Big|_{y=0,b} = D_s(Y^{(3)}_{mn} - (2-\nu_s)(\frac{m\pi}{a})^2 Y'_{mn})\Big|_{y=0,b} = 0 \qquad (16)$$

Y_{mn} and ω_{mn} can be achieved by Substituting the solution of Eq. (14) into Eq. (15) and Eq. (16) and solving the obtained homogeneous system.

Solution of Eq. (6) Can be written in the form of Eq. (11). With same X_m and Y_{mn} from homogenous solution. Substituting Eq. (11) into Eq. (6) yields:

$$
\begin{aligned}
&\sum_{m=1}^{N_x}\sum_{n=1}^{N_y} X^{(4)}_m Y_{mn}T_{mn} + 2\sum_{m=1}^{N_x}\sum_{n=1}^{N_y} X^{(2)}_m Y^{(2)}_{mn}T_{mn} + \sum_{m=1}^{N_x}\sum_{n=1}^{N_y} X_m Y^{(4)}_{mn}T_{mn} + \frac{\rho_s h_s}{D_s}\sum_{m=1}^{N_x}\sum_{n=1}^{N_y} X_m Y_{mn}\ddot{T}_{mn}\\
&\qquad = -\frac{1}{D_s}(F^z_{ts} + \sum_{k=1}^{K} F_{r_k s})
\end{aligned}
\qquad (17)
$$

Multiplying Eq. (17) By "$X_k(x)Y_{kh}(y)$" and then applying integral in the plate area yields the second-order ordinary differential equations of the plate vertical vibration in terms of the generalized coordinate $T_{mn}(t)$ as follows:

[DOI: 10.22068/IJCE.13.3.347]

$$\ddot{T}_{mn}+\frac{D_s}{\rho_s h_s}\left(\frac{B_3B_2+2B_4B_5+B_1B_6}{B_1B_2}\right)T_{mn}=$$
$$\frac{1}{\rho_s h_s B_1 B_2}\Bigg(\sum_{c=1}^{N_C}\frac{E_c A_c}{L_c}\left(C_{11}X_m(x_c)Y_{mn}(0)+C_{33}X_m(x_c)Y_{mn}(b)\right)\sin(\alpha_c)$$
$$+\sum_{c=N_C+1}^{2N_C}\frac{E_c A_c}{L_c}\left(C_{21}X_m(x_c)Y(0)+C_{43}X_m(x_c)Y_{mn}(b)\right)\sin(\alpha_c)$$
$$+\sum_{c=2N_C+1}^{3N_C}\frac{E_c A_c}{L_c}\left(C_{12}X_m(x_c)Y(0)+C_{34}X_m(x_c)Y_{mn}(b)\right)\sin(\alpha_c)$$
$$+\sum_{c=3N_C+1}^{4N_C}\frac{E_c A_c}{L_c}\left(C_{22}X_m(x_c)Y(0)+C_{44}X_m(x_c)Y_{mn}(b)\right)\sin(\alpha_c)\Bigg)$$
$$\frac{-1}{\rho_s h_s B_1 B_2}\sum_{k=1}^{K}\sum_{f=1}^{N_f}\left[K_f\left(w_s(x_f,y_{r_k},t)-w_{r_k}(x_f,t)\right)+C_f\left(\dot{w}_s(x_f,y_{r_k},t)-\dot{w}_{r_k}(x_f,t)\right)\right]X_m(x_f)Y_{mn}(y_{r_k}) \tag{18}$$

Where

$$\begin{cases} B_1=\int_0^a {X_m}^2 dx & B_2=\int_0^b {Y_{mn}}^2 dy & B_3=\int_0^a {X_m}^{(4)}X_m dx \\ B_4=\int_0^a {X_m}^{''}X_m dx & B_5=\int_0^b {Y_{mn}}^{''}Y_{mn} dy & B_6=\int_0^b {Y_{mn}}^{(4)}Y_{mn} dy \end{cases} \tag{19}$$

3.2. Tower equation of motion

Describing each tower as an Euler-Bernoulli beam, the lateral vibration of tower is given by:

$$E_t I_t\frac{\partial^4 w_{t_k}^x(x,t)}{\partial x^2}+\rho_t A_t\frac{\partial^2 w_{t_k}^x(x,t)}{\partial t^2}=\left(F_{tR_k}^x-F_{tL_k}^x\right) \tag{20}$$

in which

$$\begin{cases} F_{tR_1}^x=\sum_{c=N_C+1}^{2N_C}\frac{E_c A_c}{L_c}C_{21}\delta(x-H)\cos(\alpha_c) \\ F_{tR_2}^x=\sum_{c=3N_C+1}^{4N_C}\frac{E_c A_c}{L_c}C_{22}\delta(x-H)\cos(\alpha_c) \\ F_{tR_3}^x=\sum_{c=N_C+1}^{2N_C}\frac{E_c A_c}{L_c}C_{43}\delta(x-H)\cos(\alpha_c) \\ F_{tR_4}^x=\sum_{c=3N_C+1}^{4N_C}\frac{E_c A_c}{L_c}C_{44}\delta(x-H)\cos(\alpha_c) \end{cases} \tag{21}$$

and

$$\begin{cases} F_{tL_1}^x=\sum_{c=1}^{N_C}\frac{E_c A_c}{L_c}C_{11}\delta(x-H)\cos(\alpha_c) \\ F_{tL_2}^x=\sum_{c=N_C+1}^{3N_C}\frac{E_c A_c}{L_c}C_{12}\delta(x-H)\cos(\alpha_c) \\ F_{tL_3}^x=\sum_{c=1}^{N_C}\frac{E_c A_c}{L_c}C_{33}\delta(x-H)\cos(\alpha_c) \\ F_{tL_4}^x=\sum_{c=N_C+1}^{3N_C}\frac{E_c A_c}{L_c}C_{34}\delta(x-H)\cos(\alpha_c) \end{cases} \tag{22}$$

In order to solve the homogenous form of differential equation in Eq.(20); the solution can be expressed as:

$$w_{t_k\,l}^x=X_{t_k\,l}^x(x)\times T_{t_k\,l}^x(t) \tag{23}$$

Where

$$X_{t_k\,l}^x=A_1\cos(\beta_l x)+A_2\sin(\beta_l x)+A_3\cosh(\beta_l x)+A_4\sin(\beta_l x) \tag{24}$$

And; the boundary conditions are:

$$\begin{cases} w_{t_k}^x(0,t)=0 & \frac{\partial w_{t_k}^x(0,t)}{\partial x}=0 \\ \frac{\partial^2 w_{t_k}^x(H,t)}{\partial x^2}=0 & \frac{\partial^3 w_{t_k}^x(H,t)}{\partial x^3}=0 \end{cases} \tag{25}$$

Using Eq.(23) and boundary conditions; A_i and βl can be found. As so, Eq.(20) can be written follows:

$$E_t I_t X_{t_k\,l}^{x\,(4)}T_{t_k\,l}^x+\rho_t A_t X_{t_k\,l}^x\ddot{T}_{t_k\,l}^x=\left(F_{tR_k}^x-F_{tL_k}^x\right) \tag{26}$$

Using same method as explained in previous section, the second-order ordinary differential equation yields:

[DOI: 10.22068/IJCE.13.3.347]

$$\ddot{T}^{x}_{t_k\,l}+\frac{E_tI_t\beta_l^4}{\rho_tA_t}T^{x}_{t_k\,l}=\frac{1}{\rho_tA_tB_7}\times$$
$$[(\sum_{c=N_C+1}^{2N_C}\frac{E_cA_c}{L_c}C_{21}\delta(x-H)\cos(\alpha_c))+\sum_{c=3N_C+1}^{4N_C}\frac{E_cA_c}{L_c}C_{22}\delta(x-H)\cos(\alpha_c)$$
$$+\sum_{c=N_C+1}^{2N_C}\frac{E_cA_c}{L_c}C_{43}\delta(x-H)\cos(\alpha_c)+\sum_{c=3N_C+1}^{4N_C}\frac{E_cA_c}{L_c}C_{44}\delta(x-H)\cos(\alpha_c))$$
$$-(\sum_{c=1}^{N_C}\frac{E_cA_c}{L_c}C_{11}\delta(x-H)\cos(\alpha_c)+\sum_{c=N_C+1}^{3N_C}\frac{E_cA_c}{L_c}C_{12}\delta(x-H)\cos(\alpha_c)$$
$$+\sum_{c=1}^{N_C}\frac{E_cA_c}{L_c}C_{33}\delta(x-H)\cos(\alpha_c)+\sum_{c=N_C+1}^{3N_C}\frac{E_cA_c}{L_c}C_{34}\delta(x-H)\cos(\alpha_c))] \quad (27)$$

Where

$$B_7=\int_0^H X^{2}_{t_k\,l}dx \quad (28)$$

For analysis of vertical vibrations of tower, each tower is considered as a bar.

$$E_tA_t\frac{\partial^2w^z_{t_k}(x,t)}{\partial x^2}-\rho_tA_t\frac{\partial^2w^z_{t_k}(x,t)}{\partial t^2}=(F^z_{tR_k}+F^z_{tL_k}) \quad (29)$$

Where

$$\begin{cases}F^z_{tR_1}=\sum_{c=N_C+1}^{2N_C}\frac{E_cA_c}{L_c}C_{21}\delta(x-H)\sin(\alpha_c)\\ F^z_{tR_2}=\sum_{c=3N_C+1}^{4N_C}\frac{E_cA_c}{L_c}C_{22}\delta(x-H)\sin(\alpha_c)\\ F^z_{tR_3}=\sum_{c=N_C+1}^{2N_C}\frac{E_cA_c}{L_c}C_{43}\delta(x-H)\sin(\alpha_c)\\ F^z_{tR_4}=\sum_{c=3N_C+1}^{4N_C}\frac{E_cA_c}{L_c}C_{44}\delta(x-H)\sin(\alpha_c)\end{cases} \quad (30)$$

And

$$\begin{cases}F^z_{tL_1}=\sum_{c=1}^{N_C}\frac{E_cA_c}{L_c}C_{11}\delta(x-H)\sin(\alpha_c)\\ F^z_{tL_2}=\sum_{c=N_C+1}^{3N_C}\frac{E_cA_c}{L_c}C_{12}\delta(x-H)\sin(\alpha_c)\\ F^z_{tL_3}=\sum_{c=1}^{N_C}\frac{E_cA_c}{L_c}C_{33}\delta(x-H)\sin(\alpha_c)\\ F^z_{tL_4}=\sum_{c=N_C+1}^{3N_C}\frac{E_cA_c}{L_c}C_{34}\delta(x-H)\sin(\alpha_c)\end{cases} \quad (31)$$

The boundary conditions are:

$$\begin{cases}w^z_{t_k}(0,t)=0\\ \frac{\partial w^z_{t_k}(H,t)}{\partial x}=0\end{cases} \quad (32)$$

The solution can be expressed as:

$$w^z_{t_k}=\sum_{l=1}^{L}X^z_{t_k\,l}(x)T^z_{t_k\,l}(t)=\sum_{l=1}^{L}\sin(\frac{(2l-1)\pi}{2H}x)T^z_{t_k\,l}(t) \quad (33)$$

Substituting Eq.(33) into Eq.(29) yields:

$$[-E_tA_t(\frac{(2l-1)\pi}{2H})^2T^z_{t_k\,l}-\rho_tA_t\ddot{T}^z_{t_k\,l}]\sin(\frac{(2l-1)\pi}{2H})=F^z_{tR_k}+F^z_{tL_k} \quad (34)$$

Using same approach:

$$\ddot{T}^z_{t_k\,l}+\frac{E_t}{\rho_t}(\frac{(2l-1)\pi}{2H})^2T^z_{t_k\,l}=\frac{-1}{\rho_tA_t\frac{H}{2}}\times$$
$$[\sum_{c=N_C+1}^{2N_C}\frac{E_cA_c}{L_c}C_{21}\delta(x-H)\sin(\alpha_c)+\sum_{c=3N_C+1}^{4N_C}\frac{E_cA_c}{L_c}C_{22}\delta(x-H)\sin(\alpha_c)$$
$$+\sum_{c=N_C+1}^{2N_C}\frac{E_cA_c}{L_c}C_{43}\delta(x-H)\sin(\alpha_c)+\sum_{c=3N_C+1}^{4N_C}\frac{E_cA_c}{L_c}C_{44}\delta(x-H)\sin(\alpha_c)$$
$$+\sum_{c=1}^{N_C}\frac{E_cA_c}{L_c}C_{11}\delta(x-H)\sin(\alpha_c)+\sum_{c=N_C+1}^{3N_C}\frac{E_cA_c}{L_c}C_{12}\delta(x-H)\sin(\alpha_c)$$
$$+\sum_{c=1}^{N_C}\frac{E_cA_c}{L_c}C_{33}\delta(x-H)\sin(\alpha_c)+\sum_{c=N_C+1}^{3N_C}\frac{E_cA_c}{L_c}C_{34}\delta(x-H)\sin(\alpha_c)] \quad (35)$$

[DOI: 10.22068/IJCE.13.3.347]

3.3. Rail equation of motion

Describing each rail as an Euler-Bernoulli beam, the vertical vibration of rail is given by:

$$E_r I_r \frac{\partial^4 w_{r_k}(x,t)}{\partial x^4} + \rho_r A_r \frac{\partial^2 w_{r_k}(x,t)}{\partial t^2} = F_{sr_k} + F_{wr_k} \quad (36)$$

in which

$$F_{sr_k} = \sum_{f=1}^{N_f} [K_f (w_s(x_f, y_{r_k}, t) - w_{r_k}(x_f, t)) + C_f (\dot{w}_s(x_f, y_{r_k}, t) - \dot{w}_{r_k}(x_f, t))] \delta(x - x_f) \quad (37)$$

$$F_{wr_k} = \sum_{w=1}^{4} F_w^v \delta(x - (v_w t + L_w)) \quad (38)$$

The boundary conditions are:

$$\begin{cases} w_{r_k}(0,t) = 0 \quad \dfrac{\partial^2 w_{r_k}(0,t)}{\partial x^2} = 0 \\ w_{r_k}(a,t) = 0 \quad \dfrac{\partial^2 w_{r_k}(a,t)}{\partial x^2} = 0 \end{cases} \quad (39)$$

The solution can be determined as:

$$w_{r_k} = \sum_{l=1}^{L} X_{r_k\, l}(x) T_{r_k\, l}(t) = \sum_{l=1}^{L} \sin(\frac{l\pi}{a} x) T_{r_k\, l}(t) \quad (40)$$

Substituting Eq.(40) into Eq.(36) yields:

$$E_r I_r \sum_{l=1}^{L} X_{r_k\, l}^{(4)} T_{r_k\, l} + \rho_r A_r \sum_{l=1}^{L} X_{r_k\, l} \ddot{T}_{r_k\, l} = F_{sr_k} + F_{wr_k} \quad (41)$$

The second-order ordinary differential equations of the rail can be found as follows:

$$\ddot{T}_{r_k\, l} + \frac{E_r I_r}{\rho_r A_r} \frac{B_8}{B_9} T_{r_k\, l} = \frac{1}{\rho_r A_r B_9} \sum_{w=1}^{4} F_w X_{r_k\, l}(x - (v_w t + L_w)) + \frac{1}{\rho_r A_r B_9} \sum_{f=1}^{N_f} [K_f (w_s(x_f, y_{r_k}, t) - w_{r_k}(x_f, t)) + C_f (\dot{w}_s(x_f, y_{r_k}, t) - \dot{w}_{r_k}(x_f, t))] X_{r_k\, l}(x_f) \quad (42)$$

where

$$B_8 = \int_0^a X_{r_k\, l}^{(4)} X_{r_k\, l} dx = (\frac{l\pi}{a})^4 \frac{a}{2} \quad , \quad B_9 = \int_0^a X_{r_k\, l} X_{r_k\, l} dx = \frac{a}{2} \quad (43)$$

3.4. Equation of motion of the vehicle

Two coordinate systems are attached to the centers of masses of the model parts. One fixed to the part and rotates with it (denoted by the index "r"), and the other one is fixed at the initial position of the object (denoted by the index "o"). Also as shown in Figure 2 a coordinate system is fixed to the bridge deck as reference.

Using Figure 5, the relationship between components of an arbitrary vector in rotating and initial coordinate systems can be given as:

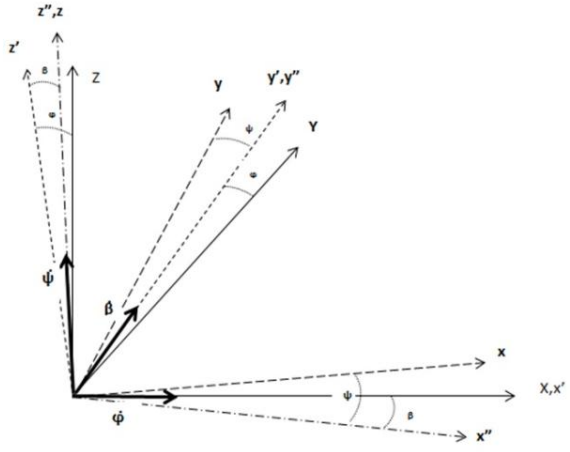

Fig. 5 Coordinate transformation

$$R_r^o = R_{x,\varphi} R_{y,\beta} R_{z,\psi} = \begin{bmatrix} 1 & 0 & 0 \\ 0 & \cos\varphi & -\sin\varphi \\ 0 & \sin\varphi & \cos\varphi \end{bmatrix} \begin{bmatrix} \cos\beta & 0 & \sin\beta \\ 0 & 1 & 0 \\ -\sin\beta & 0 & \cos\beta \end{bmatrix} \begin{bmatrix} \cos\psi & -\sin\psi & 0 \\ \sin\psi & \cos\psi & 0 \\ 0 & 0 & 1 \end{bmatrix} \quad (44)$$

[DOI: 10.22068/IJCE.13.3.347]

Also angular velocity can be obtained as:

$$\begin{aligned}\omega &= \dot{\psi}\hat{k} + \dot{\beta}\hat{j}'' + \dot{\varphi}\hat{i}' \\ &= \dot{\psi}\hat{k} + \dot{\beta}(\hat{j}\cos\psi + \hat{i}\sin\psi) + \dot{\varphi}(\hat{i}''\cos\beta + \hat{k}''\sin\beta) \\ &= \dot{\psi}\hat{k} + \dot{\beta}(\hat{j}\cos\psi + \hat{i}\sin\psi) \\ &\quad + \dot{\varphi}(\hat{i}\cos\psi\cos\beta - \hat{j}\sin\psi\cos\beta + \hat{k}\sin\beta) \\ &= (\dot{\beta}\sin\psi + \dot{\varphi}\cos\psi\cos\beta)\hat{i} + (\dot{\beta}\cos\psi - \dot{\varphi}\sin\psi\cos\beta)\hat{j} \\ &\quad + (\dot{\psi} + \dot{\varphi}\sin\beta)\hat{k}\end{aligned} \tag{45}$$

And angular accelerations are:

$$\begin{cases}\dot{\omega}^x = \ddot{\beta}\sin\psi + \dot{\beta}\dot{\psi}\cos\psi + \ddot{\varphi}\cos\psi\cos\beta - \dot{\varphi}\dot{\beta}\sin\beta\cos\psi \\ \qquad - \dot{\varphi}\dot{\psi}\cos\beta\sin\psi \\ \dot{\omega}^y = \ddot{\beta}\cos\psi - \dot{\beta}\dot{\psi}\sin\psi - \ddot{\varphi}\sin\psi\cos\beta + \dot{\varphi}\dot{\beta}\sin\beta\sin\psi \\ \qquad - \dot{\varphi}\dot{\psi}\cos\beta\cos\psi \\ \dot{\omega}^z = \ddot{\psi} + \ddot{\varphi}\sin\beta + \dot{\varphi}\dot{\beta}\cos\beta\end{cases} \tag{46}$$

For each wagon part, the equations of motion can be written as [10]:

$$\sum F^o = m\ddot{w}^o \tag{47}$$

$$\sum M^r = \frac{dH^r}{dt} = I^r\dot{\omega}^r + \omega^r \times I\ \omega^r \longrightarrow I^r\dot{\omega}^r = \sum M^r - \omega^r \times I\ \omega^r \tag{48}$$

The complete system equations are obtained by combining the equations of motions of deck, towers, rails and the wagon parts. Considering the initial conditions (wagon velocity and position), the equations of motions are solved numerically using Runge-Kutta method. In this method the system equations are converted into state variables. Both displacements and velocities at time $t + \Delta t$ are treated as unknown and then can be obtained from the information of the time *t* [11].

4. Results and Discussions

In order to study the effects of various parameters on the behavior of a vehicle–bridge interaction, Evripos bridge in Greece is chosen as a case study. The main parameters of the rails and the bridge used in the simulation are listed in Tables 4-5 [12].

Table 4 Main parameters of the track

Notation	Parameter	Value
E_r	Elastic modulus of rail	205.9 Gpa
I_r	Rail second moment of area	3.217×105 m^4
ρ_r	Rail density	7860 kg m^{-3}
A_r	Rail cross-section area	7.715×10-3 m^2
K_f	Fastener stiffness	6.5×107 N m^{-1}
C_f	Fastener damping	6.5×104 N s m^{-1}
L_f	Sleeper spacing	0.79 m
L_r	Rail gage	1.5 m
N_c	Number of cables	10

Table 5 Main parameters of the bridge

Notation	Parameter	Value
a	Bridge length	395 m
b	Bridge width	13.5 m
H_s	Deck thickness	0.45 m
H_t	Tower height	35 m
D_c	Diameter of each strand in one cable	15.24×10^{-3} m
ρ_s	Density of deck	7860 kg m^{-3}
υ_s	Poisson's ratio of deck	0.29
E_s	Deck module of elasticity	205.9 Gpa

[DOI: 10.22068/IJCE.13.3.347]

Figure 6 shows the maximum amplitude of rail vibration with respect to the lateral rail location on the bridge. According to this figure rails vibration is minimized if the rails centerline locates on the centerline of the cable bridge.

Effects of the height and cross section dimensions of the tower on maximum amplitude of deck vibration are investigated in Figure 7. The results show that with decrease in tower cross sectional area, maximum rail displacement increases. Also according to this figure there is an optimum tower height in which the maximum rail displacement will be minimum.

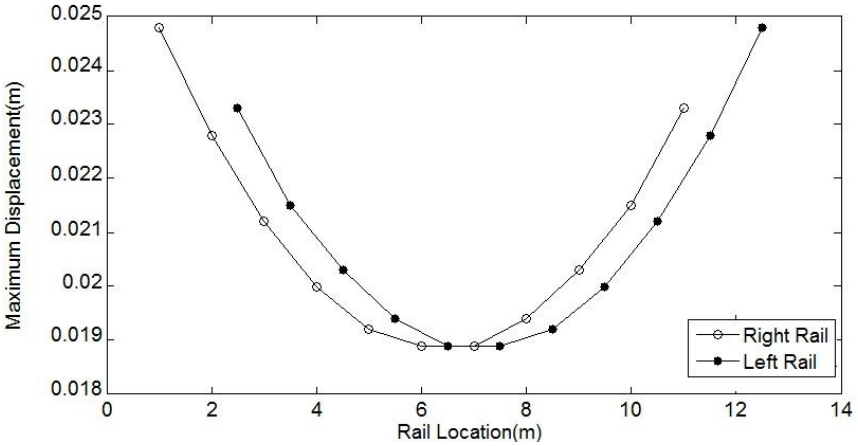

Fig. 6 Maximum amplitude of rail vibration respect to the lateral rail location

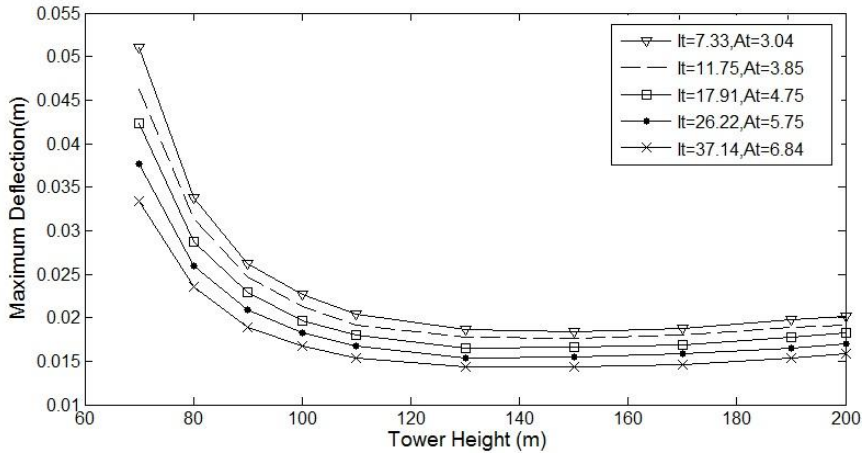

Fig. 7 Effects of tower height on maximum displacement of rail

Effects of number of cables and number of strands in each cable on maximum displacement of rail are shown in Figure 8. The results show that with increase of these parameters the rail displacement decrease and the bridge become more rigid.

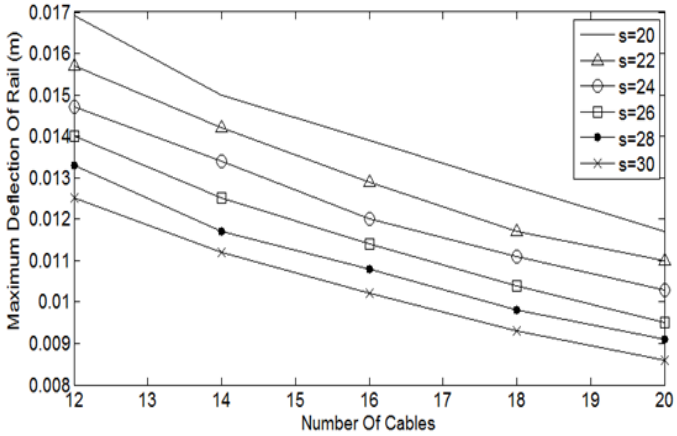

Fig. 8 Effects of number of cables and number of strands in each cable on maximum displacement of rail

[DOI: 10.22068/IJCE.13.3.347]

Vertical displacement of the rail and Vertical position of wagon center of mass when the train passes over the bridge are presented in Figures 9 and 10, respectively. According to these figures maximum vibration of wagon position and rail displacement occur when the wagon reaches the middle of the bridge.

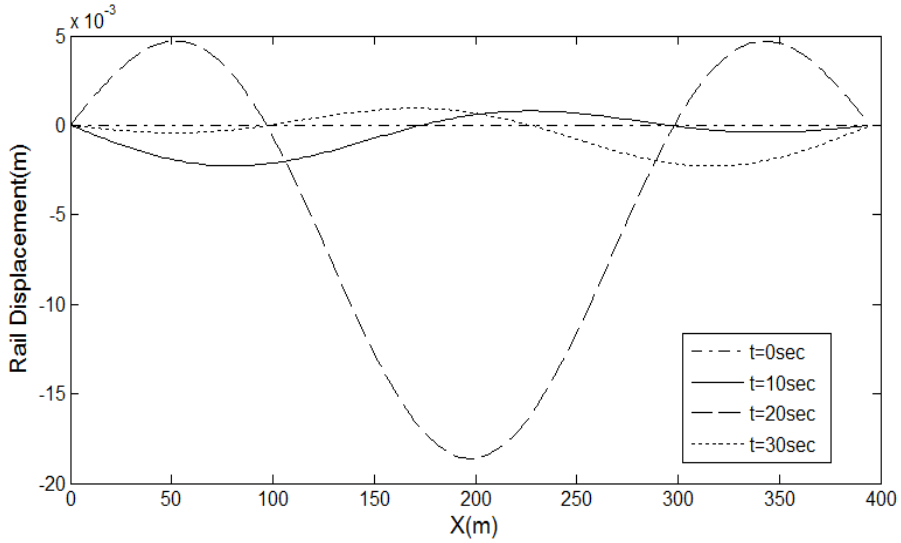

Fig. 9 Vertical displacement of rail

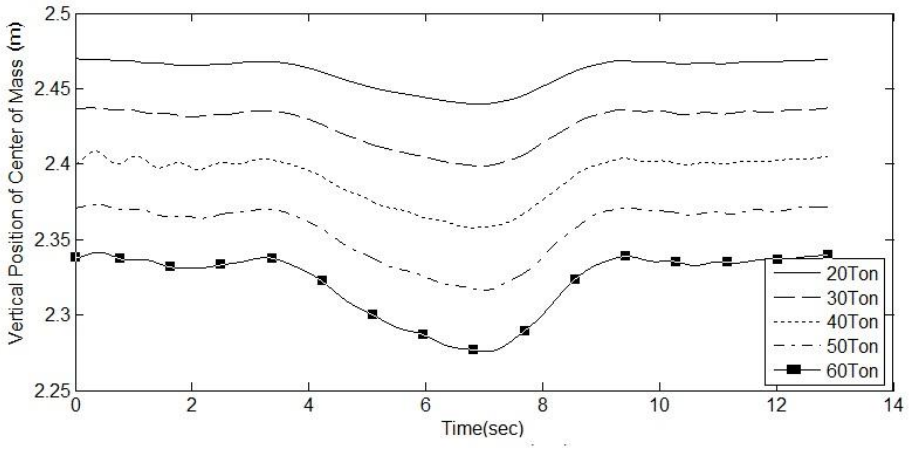

Fig. 10 Vertical position of wagon center of mass

The comfort of the passenger coach in a running train can be assessed using the Sperling factor defined as:

$$Sperling \quad factor = 0.896\left(\frac{\ddot{w}_{wg}^{z}\,(cm/s^2)^3}{f}F(f)\right) \qquad (49)$$

Where f is the frequency in Hz; and F(f) is the modification coefficient of frequency. When vertical vibration is concerned,

$$F(f)=\begin{cases}0.325 & 0.5<f<5.9\\ \dfrac{400}{f^2} & 5.9<f<20\\ 1 & f>20\end{cases} \qquad (50)$$

The allowable value of vehicle comfort is 3.0 for vertical vibrations [3].

The acceleration response of the car body is random due to random rail irregularities and it contains a wide range of vibration frequencies. Thus, the Sperling comfort index is calculated for a series of frequencies based on the Fourier spectrum of the acceleration response time history. Acceleration response of the car body for different wagon speeds and line grades is presented in Figures 11 and 12.

Using these results Sperling comfort index is calculated and presented in Figure 13. It can be seen that the Sperling index is less than 2, indicating that the ride comfort is satisfactory.

[DOI: 10.22068/IJCE.13.3.347]

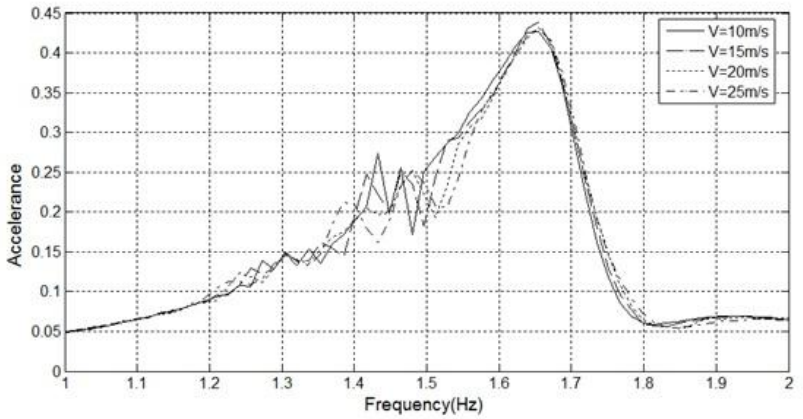

Fig. 11 Acceleration response of the car body for different wagon speeds

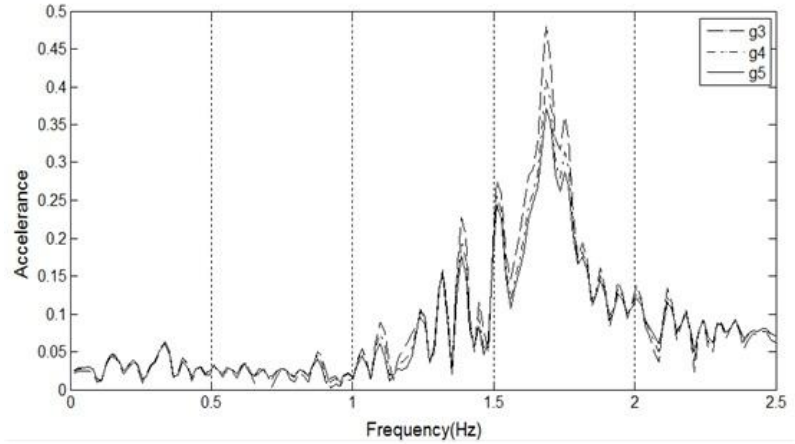

Fig. 12 Acceleration response of the car body for different line grades

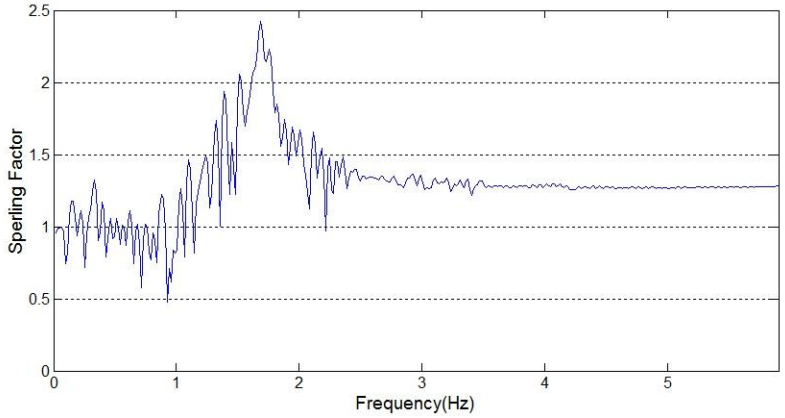

Fig. 13 Sperling comfort index of the car body

5. Validation of the model

Example 1: To validate the model illustrated in this paper its predictions of the responses are compared with the responses are reported by Xu et al. [3] for the case where there are no cross wind forces. The vertical displacement response of bridge girder at mid-span evaluated by the current model and that of presented Xu et al. [3] are shown in Figures 14(a) and (b) respectively. According to these figures, the difference of the maximum amplitudes of the two results is about 5.5%. Therefore the prediction of the responses by the current model is in good agreement with the responses reported by Xu et al. [3].

Example 2: Yau and Yang [2] reported their results of the finite element simulation on the study of vertical interaction between the high speed trains and the cable bridges. In this research the train has been modeled as a series of sprung masse, the bridge deck and towers by nonlinear beam-column elements, and the stay cables by truss elements with Ernst's equivalent modulus. Using the finite element procedure, the impact factor *I* has been

[DOI: 10.22068/IJCE.13.3.347]

solved for the midpoint of the arrival span and departure span of the cable-stayed bridge. Figures 15 show the comparison of the impact factor *I* with respect to the speed parameter *S* from the reference and the calculated impact factor using the current model. It can be seen from Figures 15(a) and (b), that the numerical results predicted by the present model are in reasonable agreement with the results calculated by finite element method.

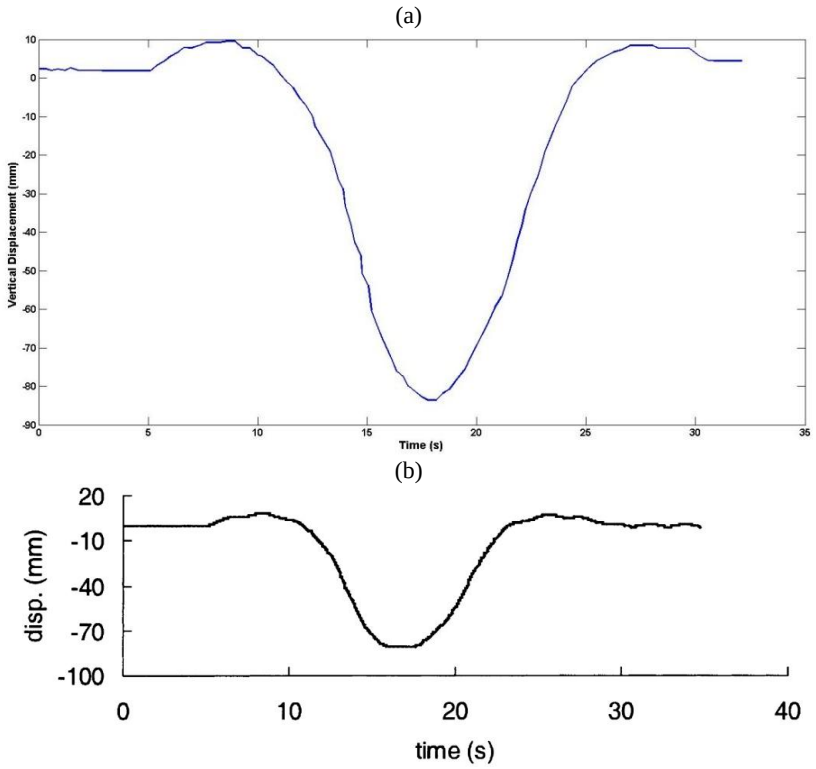

Fig. 14 Vertical displacement response of bridge girder at mid-span

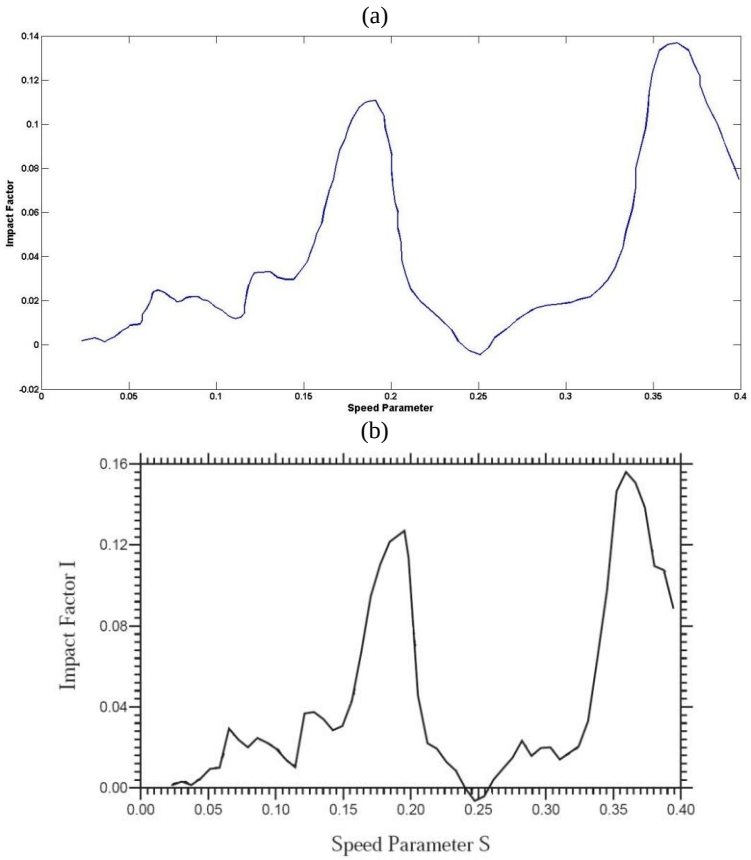

Fig. 15 Impact factor of the cable-stayed bridge

[DOI: 10.22068/IJCE.13.3.347]

Example 3: The model developed by Au et al. [1] has been used for validation of the dynamic model of wagon and bridge interaction as reported in this paper. In that paper, the impact factor of deck moment was obtained using 2D model analyzed by the FEM. Figure 16 shows the comparison of the impact factor calculated using the current model with the results presented by Au et al. [1]. According to this figure the magnitude of the impact factor of the current model has a certain deviation compared with the values obtained by Au et al. [1] and the maximum error is about 5.8%.

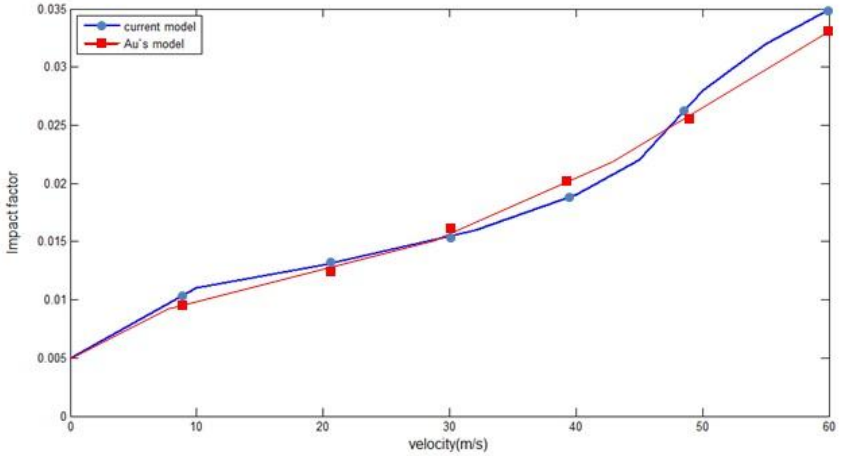

Fig. 16 Comparison of the impact factor for 2D and 3D models

6. Conclusion

In this paper a 3-D nonlinear models of cable bridge and wagon have been used to investigate the interaction of the cable bridge and train system. The current model has been validated using several numerical models reported in the literature by other researchers. Using this model; the effects of wagon velocity, lateral position of the rails and rail irregularities on wagon/bridge vibration and passenger comfort have been studied.

List of Symbols

A	Cross section area	α	Geometric slope
C	Fastener damping in vertical direction	υ	Poisson's ratio
D	Flexural rigidity	ρ	Density
E	Module of elasticity	ω	Angular velocity
F	Force	$(\,)^r$	Relative frame
H	Tower height	$(\,)^x$	Horizontal direction
I	Second moment of area	$(\,)^y$	Lateral direction
K	Fastener stiffness in vertical direction	$(\,)^z$	Vertical direction
L	Length or distance between different elements	$(\,)_b$	bogie
N	Number of.	$(\,)_c$	C^{th} cable
a	Bridge length	$(\,)_f$	F^{th} fastener
b	Bridge width	$(\,)_k$	K^{th} rail or tower
d	Diameter of.	$(\,)_o$	Initial frame
h	Deck thickness	$(\,)_r$	Rail
m	Mass	$(\,)_{tR}$	Right side of tower
v	Velocity	$(\,)_{rs}$	Rail to bridge deck
w	Displacement	$(\,)_{rw}$	Rail to wheel
$(\,)_s$	Bridge deck	$(\,)_{ts}$	Tower to bridge deck
$(\,)_{sr}$	Bridge deck to rail	$(\,)_w$	W^{th} wheel set
$(\,)_{st}$	Bridge deck to tower	$(\,)_{wg}$	Wagon
$(\,)_t$	Tower	$(\,)_{wr}$	Wheel to rail
$(\,)_{tL}$	Left side of tower		

References

[1] Au FTK, Wang JJ, Cheung YK. Impact study of cable-stayed railway bridges with random rail irregularities, Engineering Structures, 2001, Vol. 24, pp. 529-541.

[2] Yau JD, Yang YB. Vibration reduction for cable-stayed bridges traveled by high-speed trains, Finite Elements in Analysis and Design, 2004, Vol. 40, pp. 341-359.

[3] Xu YL, Zhang N, Xia H. Vibration of coupled train and cable-stayed bridge systems in cross winds, Engineering Structures, 2004, Vol. 26, pp. 1389-1406.

[DOI: 10.22068/IJCE.13.3.347]

[4] Yang YB, Wu YS. Dynamic stability of trains moving over bridges shaken by earthquakes, Journal of Sound and vibration, 2002, Vol. 258, pp. 65-94.
[5] Jalili MM, Salehi H. Wheel/rail contact model for rail vehicle dynamics, Comptes Rendus Mecanique, 2011, Vol. 339, pp. 700-707.
[6] Durali M, Jalili MM. A New criterion for assessment of train derailment risk, Proc. IMechE Part K: Journal of Multi-Body Dynamics, 2011, Vol. 224, pp. 83-101.
[7] Iyengar RN, Jaiswal OR. Random Field modeling of railway track irregularites, Journal of Transportation Engineering,1995, pp. 303-308.
[8] Fryba L. Dynamics of railway bridges, Thomas Telford, London, 1996.
[9] Xiang Y, Zhao YB, Wei GW. Levy solutions for vibration of multi-span rectangular plates, International Journal of Mechanical Sciences, 2002, Vol. 44, pp. 1195-1218.
[10] Durali M, Shadmehri B. Nonlinear analysis of train derailment in severe braking, Journal of Dynamic Systems, Measurement, and Control, 2003, Vol. 125, pp. 48-53.
[11] Garg VK, Dukkipati RV. Dynamics of Railway Vehicle Systems, Academic Press, Canada, 1984.
[12] Virlogeux M. Recent evolution of cable stayed bridges, Engineering Structures, 1999, Vol. 21, pp. 737-755.

[DOI: 10.22068/IJCE.13.3.347]